Molecular Cell, Vol. 10, 295–305, August, 2002, Copyright ©2002 by Cell Press

X-Ray Crystal Structure and Functional Analysis of Vaccinia Virus K3L Reveals Molecular Determinants for PKR Subversion and Substrate Recognition

Arvin C. Dar[1,2] and Frank Sicheri[1,2,3]
[1]Program in Molecular Biology and Cancer
Samuel Lunenfeld Research Institute
Mount Sinai Hospital
600 University Avenue
Toronto, Ontario M5G 1X5
[2]Department of Molecular and Medical Genetics
University of Toronto
Toronto, Ontario M5S 1A8
Canada

Summary

The vaccinia virus protein K3L subverts the mammalian antiviral defense mechanism by inhibiting the RNA-dependent protein kinase PKR. K3L is a structural mimic of PKR's natural substrate, the translation initiation factor eIF2α. To further our understanding of K3L inhibitory function and PKR substrate recognition, we have solved the 1.8 Å X-ray crystal structure of K3L. The structure consists of a five-strand β barrel with an intervening helix insert region similar in topology to the functionally divergent S1 domain. Mutational analysis identifies two proximal regions of the K3L structure as possessing specialized PKR binding and inhibitory function. Further analysis reveals that PKR dimerization composes a key switch that regulates both its catalytic activation and its molecular recognition of K3L and eIF2α.

Introduction

The double-stranded RNA-dependent protein kinase (PKR) plays an integral role in the innate immunity to viral infection. In response to the detection of viral products within a host organism, PKR initiates signaling cascades that limit the replicative capacity of virus within the cell and induce the expression and release of interferon α and β to raise a heightened antiviral state in cells not yet infected (reviewed in Stark et al., 1998). Like other members of the eIF2α family of Ser/Thr protein kinases, PKR regulates protein synthesis in response to cellular stress through the phosphorylation of the α subunit of the eukaryotic protein translation initiation factor, eIF2 (reviewed in Dever, 2002). Phosphorylated eIF2α arrests protein synthesis by sequestering the rate-limiting component of the translation machinery, the guanine nucleotide exchange factor eIF2B. While activated by distinct stress stimuli, each eIF2α protein kinase phosphorylates eIF2α at the identical residue, serine 51, suggesting a common mode of substrate recognition and downstream mechanism of phosphoregulation.

Substrate recognition plays a critical role in imparting specificity to a protein kinase signaling response, and the poor comprehension of this aspect of protein kinase function has been a major impediment to accurately mapping the signaling pathways that govern cellular behavior. To date, substrate recognition by protein kinases has been shown to occur by a variety of mechanisms encoded by the protein kinase catalytic domain itself and by neighboring domains or intermolecular subunits in multidomain and multisubunit protein kinases, respectively. Through interactions involving its active site region, the protein kinase domain possesses a limited capacity to discriminate phosphorylation sites, serine/threonine, or tyrosine residues in short sequence contexts (reviewed in Johnson et al., 1998). This measure of specificity however is most often augmented by additional mechanisms of recognition involving secondary interactions between a substrate and the peripheral regulatory domains or subunits of the protein kinase.

The recognition of eIF2α by PKR and by the eIF2α protein kinases in general is dictated primarily by determinants within their catalytic domains. Indeed, the eIF2α protein kinases PKR, yeast GCN2, heme-regulated eIF2α kinase (HRI), and the pancreatic eIF2α kinase (PEK) share sequence similarity only within their catalytic domains, and in the case of PKR, its catalytic domain is sufficient for propagating a translational inhibitory response in vivo (Ung et al., 2001; Vattem et al., 2001a). Contrary to expectation, substrate recognition by the eIF2α protein kinases is directed toward regions removed from the site of phosphorylation in eIF2α. In fact, a peptide derived from the Ser51 phosphorylation site of eIF2α is a poor PKR substrate, in comparison to the full-length protein ($K_m$peptide = 1.08 mM and K_meIF2α = 0.626 μM) (Mellor and Proud, 1991). Further insight into PKR's substrate recognition mechanism has been gleaned from studies of a PKR subversive product encoded by the vaccinia virus.

Vaccinia virus encodes the protein, K3L, which confers interferon resistance and maintains viral replication and protein translation within infected cells (Beattie et al., 1991, 1995). K3L has been shown to suppress PKR activation and eIF2α phosphorylation in mammalian cells (Davies et al., 1992), in a heterologous yeast system (Kawagishi-Kobayashi et al., 1997), and in vitro using semipurified recombinant proteins (Carroll et al., 1993; Davies et al., 1993). Yeast two hybrid and in vitro binding experiments have shown the interaction between K3L and the catalytic domain of PKR to be direct (Cosentino et al., 1995; Craig et al., 1996; Gale et al., 1996; Sharp et al., 1997). Competition binding experiments and strong sequence homology between K3L and the N-terminal third of eIF2α (72% similarity and 28% identity; see alignment in Figure 1) suggest that PKR recognizes K3L and eIF2α by a common mechanism (Sharp et al., 1997). This has led to the description of K3L as a pseudosubstrate inhibitor. This description is further supported by K3L's ability to inhibit eIF2α phosphorylation by other eIF2α protein kinases, including yeast GCN2, HRI, and PEK (Carroll et al., 1993; Qian et al., 1996; Sood et al., 2000).

In order to further our understanding of the molecular basis of PKR subversion by K3L and, by extension, the mechanism of eIF2α substrate recognition by PKR, we

[3]Correspondence: sicheri@mshri.on.ca

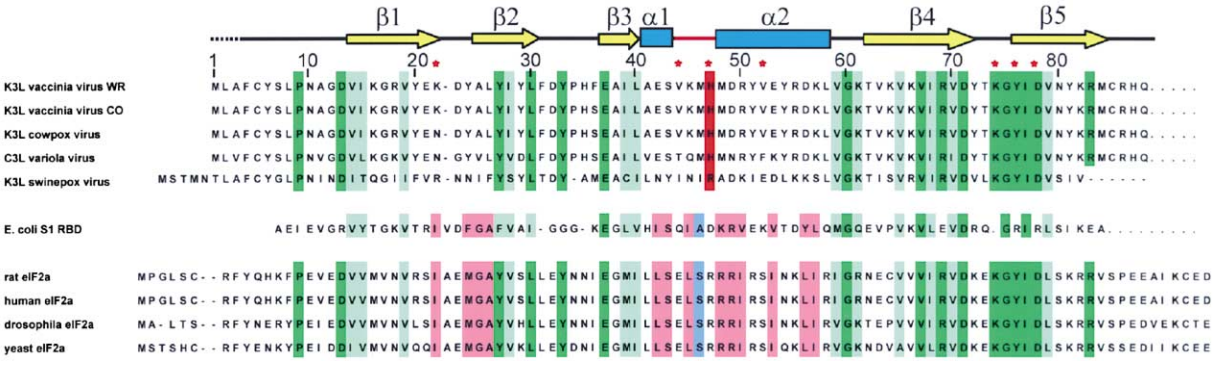

Figure 1. Structure-Based Sequence Alignment of K3L, the Amino-Terminal Third of eIF2α, and the S1 RBD

Secondary structure elements of K3L are indicated with β sheets in yellow, α helices in blue, and the connecting segment in the helical insert region in red. Invariant and highly conserved residues among K3L and eIF2α are colored dark and light green, respectively. Serine 51, the PKR phosphoregulatory site in eIF2α is colored blue. Residues conserved between eIF2α and the S1 RBD in the β1-β2 linker and the helical insert region are colored pink. In K3L, His 47 in red, denotes the apex of the helical insert region displayed in Figures 2A and 3. K3L residues identified in this report or reported previously (Kawagishi-Kobayashi et al., 1997) as important for PKR inhibitory function are denoted by red stars.

have solved the X-ray crystal structure of K3L. Using site-directed mutagenesis, binding, and detailed enzyme kinetic analyses, we have probed the functional relevance of two distinct regions of the K3L structure. The results reveal a paradigm for substrate/pseudosubstrate recognition by a protein kinase and unexpectedly a coupling mechanism between PKR substrate recognition and catalytic activation.

Results

K3L Structural Analysis

The 10.5 kDa vaccinia virus protein K3L, Wisconsin strain, was expressed and purified as previously described (Carroll et al., 1993) with modification (see Experimental Procedures). Crystals of the space group C2 (a = 73.0 Å, b = 49.6 Å, c = 59.9 Å, α = γ = 90°, β = 100.5°) with two molecules in the asymmetric unit were employed for the structure determination. The K3L structure was solved using the selenomethionine multiwavelength anomalous dispersion (MAD) phasing method and refined to 1.8 Å resolution to an R_{factor}/R_{free} of 23.2%/25.6%. Pertinent structure determination and refinement statistics are presented in Table 1. No significant structural differences between the two protein molecules in the asymmetric unit are apparent (rmsd = 0.56 Å), and both molecules are highly structured. A structure based sequence alignment of K3L, eIF2α, and the S1 RNA binding domain (S1 RBD) from *E. coli* polynucleotide phosphorylase is presented in Figure 1. A ribbon depiction of the K3L structure is shown in Figure 2A.

The crystal structure of K3L consists of a monomeric five-strand, antiparallel β barrel. Strands β1–β3 form the larger of two β sheets, while strands β4 and β5 form the smaller sheet. The interaction angle between sheets is approximately 90°. Inserted between β strands 3 and 4 is a single turn 3_{10} helix followed by a structured connecting segment of 4 amino acids and then an 11 residue right hand α helix. We refer to these three elements collectively as the helical insert region. The topology of the K3L structure is most similar to that of the functionally unrelated S1 RBD (see Figure 2B; rmsd = 2.6 Å over 63 aligned residues) (Bycroft et al., 1997), which confirms the prediction of a common fold based on sequence similarity (<15% identity) (Gribskov, 1992). The largest structural differences between K3L and the S1 RBD locate to the N and C termini, β strand 3, the β1-β2, β2-β3, and the β4-β5 connecting segments, and most notably, the secondary structure elements within the helix insert region. Within the latter, a 3_{10} helix is present in both K3L and the S1 RBD but are oriented differently with respect to the overall β structure (deviation angle between helices ≅ 125°). In addition, the connecting segment is 3 amino acid residues longer in the S1 RBD and deviates by as much as 9 Å between comparable positions in the two structures (Cα of Asp40 in S1 RBD versus Cα of Met46 in K3L). Lastly, helix 2 in the S1 RBD is composed of a single turn but adopts an

Table 1. Data Collection, Structure Determination, and Refinement Statistics

	Peak	Inflection	Remote
Wavelength (Å)	0.9788	0.9790	1.0000
Resolution (Å)	2.26	2.37	1.83
R_{sym} (%)	7.9	9.1	6.6
Total Reflections	170,730	148,014	337,368
Unique Reflections	12,629	10,939	23,042
Completeness (%)	99.8	99.9	99.8
I/σ	4.3	4.2	6.3
Phasing Power	2.3	2.6	0.91
Refinement			
Resolution range (Å)	500–1.8		
Reflections	19,455		
R_{factor}/R_{free} (%)	23.2/25.6		
Rms deviations			
Bonds (Å)	0.005		
Angles (°)	1.290		

Space group C2: a = 73.0 Å, b = 49.6 Å, c = 59.9 Å; α = γ = 90°, β = 100.5°; two molecules per asymmetric unit.

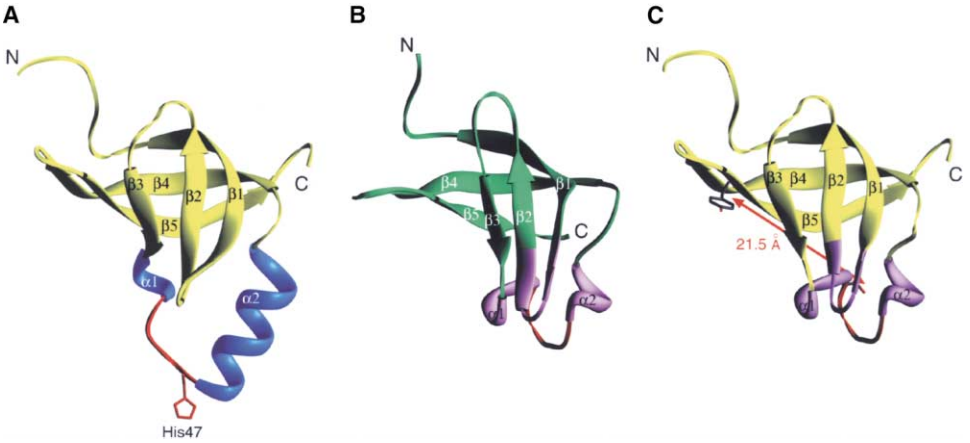

Figure 2. Structural Similarities between K3L, the S1 RBD, and eIF2α

(A) Ribbon diagram of K3L. β sheets, α helices, and the linker between α1 and α2 are colored yellow, blue, and red, respectively.

(B) Ribbon diagram of the S1 RNA binding domain of *E. coli* polynucleotide phosphorylase (Protein Data Bank ID code 1SRO) (Bycroft et al., 1997). β sheets, α helices, and the linker between α1 and α2 are colored green, pink, and red, respectively. The S1 RNA binding domain is oriented such that the antiparallel β barrel fold is aligned with the corresponding portion of K3L in (A).

(C) Hybrid model of the amino-terminal region of eIF2α composed of the antiparallel β barrel core of K3L and the β1-β2 linker and helical insert region of the S1 RBD. The 21.5 Å distance from the center of the substrate recognition motif (Tyr76) to the Ser 51 phospho-regulatory site provides a constraint for localizing the complementary binding sites in PKR.

orientation similar to the longer helix 2 in K3L. Based on sequence similarity between K3L, the S1 RBD and the amino-terminal region of eIF2α, eIF2α is predicted to closely resemble the β sheet structure of K3L, but over the helical insert region, is predicted to more closely resemble the S1 RBD structure (discussed below). The crystal structure of a proteolytic fragment of human eIF2α containing the β barrel portion but lacking the helix insert region confirms part of this prediction (Nonato et al., 2002).

PKR Recognition Motif

Projection of K3L/eIF2α invariant residues onto the K3L surface reveals a focal point of conservation (SA = 523.4 Å^2) and a number of dispersed positions (Figure 3). Dispersed positions include Pro9, Asp13, Leu30, Tyr33, Gly60, and Arg83. These residues appear to stabilize the overall protein fold by contributing to the hydrophobic core or to β turn and helix capping structures. Residues located within the focused site of conservation include Tyr27 in β strand 2 and Glu37 in β strand 3; Val67, Arg69, and Asp71 in β strand 4; and Lys74 to Asp78 in β strand 5. Of these residues, Val67 and Ile77 side chains contribute to the hydrophobic core, while Tyr27, Glu37, Arg69, Asp71, Lys74, Tyr76, and Asp78 are solvent exposed. Sequence conservation with the functionally divergent S1 RBD identifies Glu37 and Asp71 as probable determinants of the overall protein fold. Of the remaining five residues, Lys74, Tyr76, and Asp78 have been implicated in K3L's PKR inhibitory function (Kawagishi-Kobayashi et al., 1997). Based on sequence conservation and published mutagenesis data, we have termed the conserved surface centered on Tyr76, the PKR recognition motif.

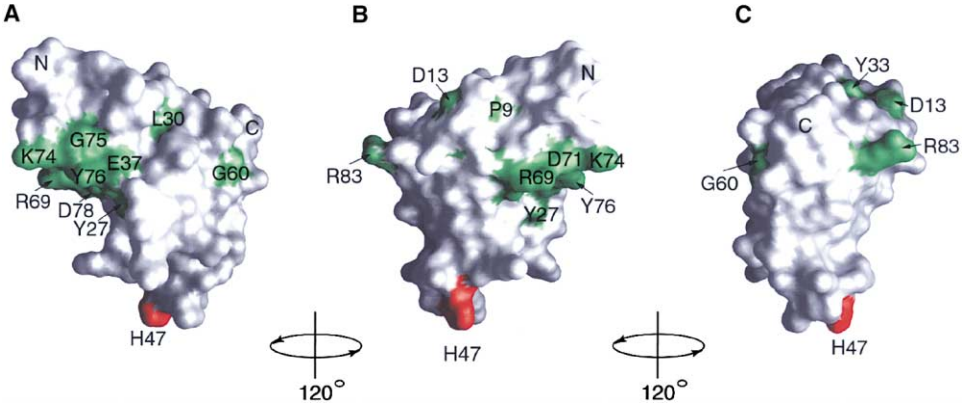

Figure 3. Conserved PKR Recognition Motif in K3L

The molecular surface of K3L is shown with K3L/eIF2α invariant residues colored green and the apex of the helical insert region, His 47, colored red. The orientation of K3L in (A) is identical to that in Figure 2A. (B) and (C) are rotations of (A) by 120° and by 240° about the vertical axis, respectively. All molecular surface and worm representations were generated using GRASP (Nicholls et al., 1991).

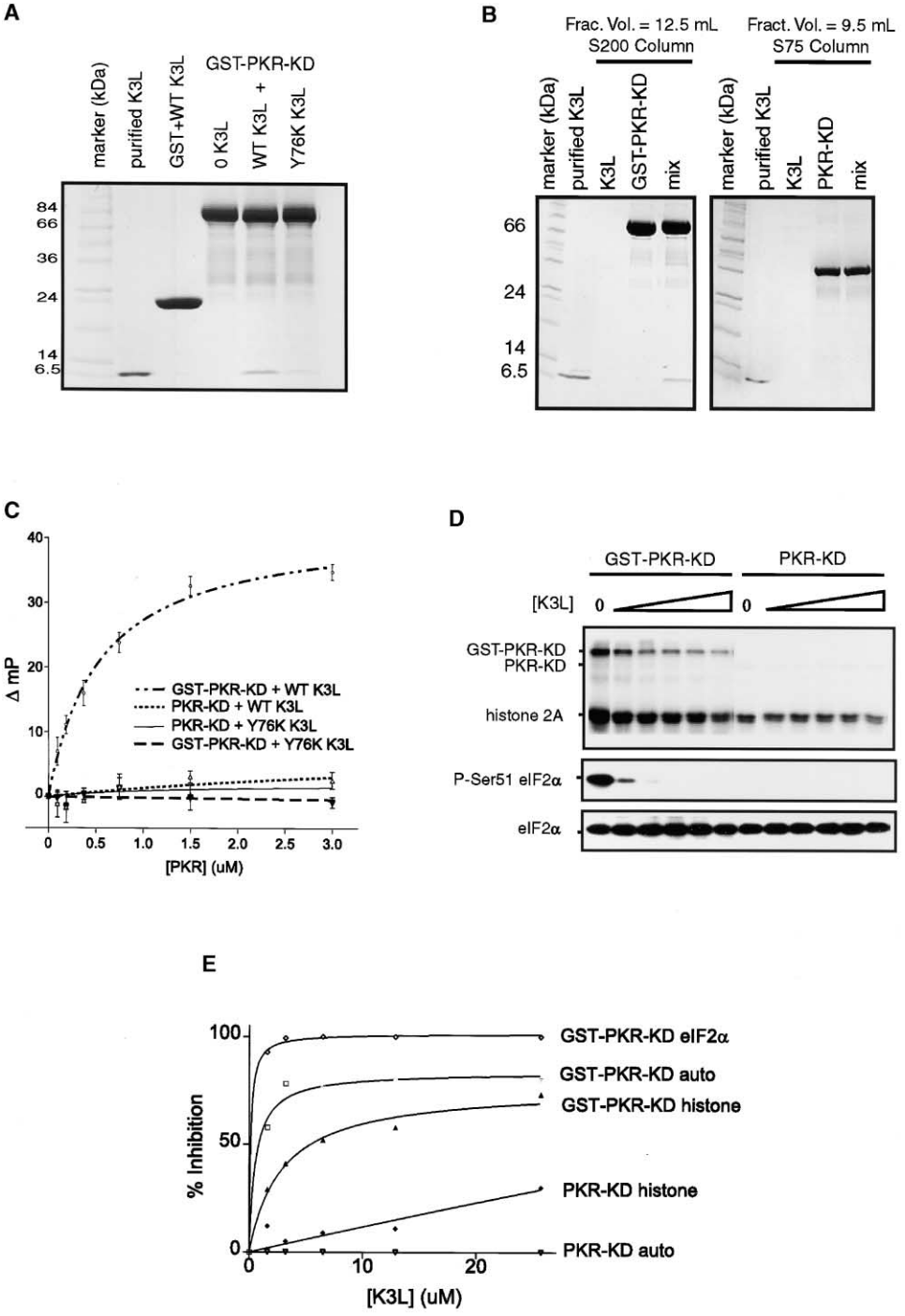

Figure 4. K3L Binds and Inhibits the GST-PKR-KD Dimer but Not the PKR-KD Monomer

(A) GST-PKD-KD pull-down assay. Wild-type (WT) K3L and the Tyr76Lys K3L mutant were incubated with GST-PKR-KD or GST bound to glutathione sepharose as indicated, washed, and then subjected to SDS-PAGE analysis and coomassie staining. Band intensity of retained K3L was quantitated with Image Quant v5.0 software. GST-PKR-KD binds selectively to wild-type K3L.

(B) Size exclusion chromatography coelution assay. 20 μM amounts of purified K3L, GST-PKR-KD, or PKR-KD alone, and mixtures of K3L with GST-PKR-KD or K3L with PKR-KD were applied to Superdex S200 or S75 gel filtration columns. Fractions corresponding to the elution volumes of the PKR proteins are shown. K3L coeluted with GST-PKR-KD only.

(C) Fluorescence polarization binding assay. 50 nM amounts of fluorescein-labeled wild-type K3L or a Tyr76Lys K3L mutant were incubated with varying amounts of GST-PKR-KD or PKR-KD as indicated. Presented are the fluorescence polarization values (ΔmP) as a function of PKR concentration. ΔmP was determined as the difference between normalized polarization values of binding reactions carried out in the absence and presence of 100-fold molar excess unlabeled K3L. A curve indicative of binding is only apparent upon addition of GST-PKR-KD to wild-type K3L.

(D) In vitro kinase assay. 0.5 μM amounts of GST-PKR-KD or PKR-KD were incubated with γ^{32}P ATP; histone 2A; and 0, 3.2, 6.4, 12.9, or 25.7

Helix Insert Region

The PKR phosphoregulatory site in eIF2α implicated in translational control projects to the connecting segment between helix 1 and 2 in the K3L and S1 RBD structures (see sequence alignment Figure 1). The area of greatest sequence dissimilarity between K3L and eIF2α encompasses the helix insert region, where interestingly sequence conservation between eIF2α and the S1 RBD is high. In the K3L structure, apolar residues in the helix insert region including Met 46, Tyr51, Tyr54, and Leu58 together with apolar residues Tyr20, Ala 25, and Leu26 in the β1-β2 linker form an extension of the β barrel hydrophobic core.

In the S1 RBD structure, a hydrophobic core extension is also observed involving the apolar residues Ile35, Ile38, Val 43, Val 46, Tyr49, and Leu50 in the helix insert region and Ile16 and Ala21 in the β1-β2 linker. All 8 apolar residues and the length of the β1-β2 linker are highly conserved between eIF2α homologs and the S1 RBD but not K3L homologs. Interactions in the hydrophobic core extension appear to dictate the specific orientation of helix 1, helix 2, and the intervening segment that distinguishes the S1 RBD and K3L structures. These observations lead us to predict that eIF2α will adopt an S1 RBD-like conformation over the helix insert region and the β1-β2 connecting segment. However, over all other regions of its structure, conservation of primary structure leads us to predict that eIF2α will more closely resemble K3L than the S1-RBD. A hybrid model of eIF2α illustrating the structural similarities with K3L and the S1 RBD is shown in Figure 2C.

The functional significance of the structural difference between K3L and eIF2α over the helix insert region has not been thoroughly explored but could be expected to relate to K3L's function as a PKR inhibitor versus eIF2α's function as a physiological substrate. This would imply that the helical insert region of K3L might serve a PKR inhibitory function. Consistent with this hypothesis, a His47Arg mutation in the helix 1-helix 2 connecting segment was previously shown to increase K3L inhibitory function in vivo (Kawagishi-Kobayashi et al., 1997).

Kinetic Characterization of K3L Inhibitor Function

We have performed a detailed characterization of the PKR binding and inhibitory function of wild-type K3L. For these analyses, we employed a glutathione S-transferase-PKR kinase domain (residues 242–551) fusion (GST-PKR-KD) expressed in *E. coli*. Due to expression problems relating to the robust catalytic activity of GST-PKR-KD, we utilized a kinase domain point mutant (His412Asn) identified serendipitously while subcloning. The His412Asn mutation, which lies deep in the catalytic cleft in close proximity to the catalytic base Asp414, attenuates catalytic function without abolishing the binding of ATP and peptide substrates. GST-PKR-KD expressed to high levels in bacteria and was purified to homogeneity using glutathione sepharose and size exclusion chromatography. Consistent with the dimeric structure of GST (McTigue et al., 1995), the GST-PKR-KD fusion eluted as a dimer during size exclusion chromatography (141.0 kDa elution mass versus 134.7 kDa calculated mass for a dimer). In contrast, the isolated kinase domain obtained by cleavage of GST-PKR-KD with TEV protease behaved as a monomer (36.2 kDa elution mass versus 44.7 kDa calculated mass for a monomer). We find that the GST-PKR-KD dimer is 8- to 10-fold more active than the PKR-KD monomer as assessed by histone, peptide, and autophosphorylation (Figure 4D, lane 1 versus 7; and Figures 5A and 5B). This observation is consistent with the reported sufficiency of dimerization for PKR signaling in vivo (Ung et al., 2001; Vattem et al., 2001a).

To verify the function of GST-PKR-KD we first tested its ability to bind K3L in a pull-down assay (Figure 4A). Incubation of GST-PKR-KD bound to glutathione sepharose with wild-type K3L, followed by washing and analysis by SDS-PAGE indicated retention of K3L. Retention of K3L on GST bound to glutathione sepharose was not detectable. As a control, we generated a Tyr76Lys mutant of K3L and tested its ability to bind GST-PKR-KD. Previously, a Tyr76Ala mutation was shown to compromise K3L inhibitory function on PKR in a heterologous yeast system (Kawagishi-Kobayashi et al., 1997). As expected, binding of the Tyr76Lys mutant to GST-PKR-KD was drastically reduced (<90%) relative to wild-type K3L, confirming that Tyr76 is essential for binding. Together these results indicate that the binding interaction between PKR and K3L can be recapitulated with our GST-PKR-KD construct.

To further probe the binding interaction between PKR and K3L, we tested for complex formation using size exclusion chromatography. As indicated by coelution, K3L binds to GST-PKR-KD, but interestingly, not to PKR-KD (Figure 4B). This observation is corroborated by fluorescence polarization studies using fluorescein-labeled K3L (Figure 4C). A robust change in polarization signal consistent with binding is observed upon addition of GST-PKR-KD to labeled K3L (K_d = 0.55 μM). In contrast, evidence of binding was not observed upon addition of PKR-KD to fluorescein-labeled K3L or upon the addition of either GST-PKR-KD or PKR-KD to a fluorescein-labeled Tyr76Lys K3L mutant.

We then performed an in vitro ^{32}P-ATP kinase labeling reaction using histone-2A as a substrate (Figure 4D). Histone-2A was previously shown to be a good in vitro substrate for PKR (Hovanessian and Kerr, 1979). GST-PKR-KD and PKR-KD were incubated with histone-2A and varying concentrations of K3L. Autophosphorylation and histone phosphorylation were then visualized

μM of K3L as indicated. Following SDS-PAGE, gels were dried and visualized by phosphor imaging (top panel). In separate reactions, 0.5 μM amounts of GST-PKR-KD or PKR-KD were incubated with 500 μM ATP; recombinant His-tagged eIF2α (residues 8–93); and 0, 3.2, 6.4, 12.9, or 25.7 μM of K3L as indicated. eIF2α phosphorylation was detected using an anti-phospho-Ser51-eIF2α antibody (middle panel), and the amount of total eIF2α was examined using anti-His antibody (lower panel).

(E) Integrated intensities corresponding to GST-PKR-KD and PKR-KD autophosphorylation, histone 2A phosphorylation, and eIF2α phosphorylation in (C). γ^{32}P ATP incorporation was quantified using ImageQuant v5.0 software, and eIF2α phosphorylation was quantitated using Quantity One v4.2 software. For percent inhibition, reaction rates were normalized versus the reaction rate in the absence of K3L.

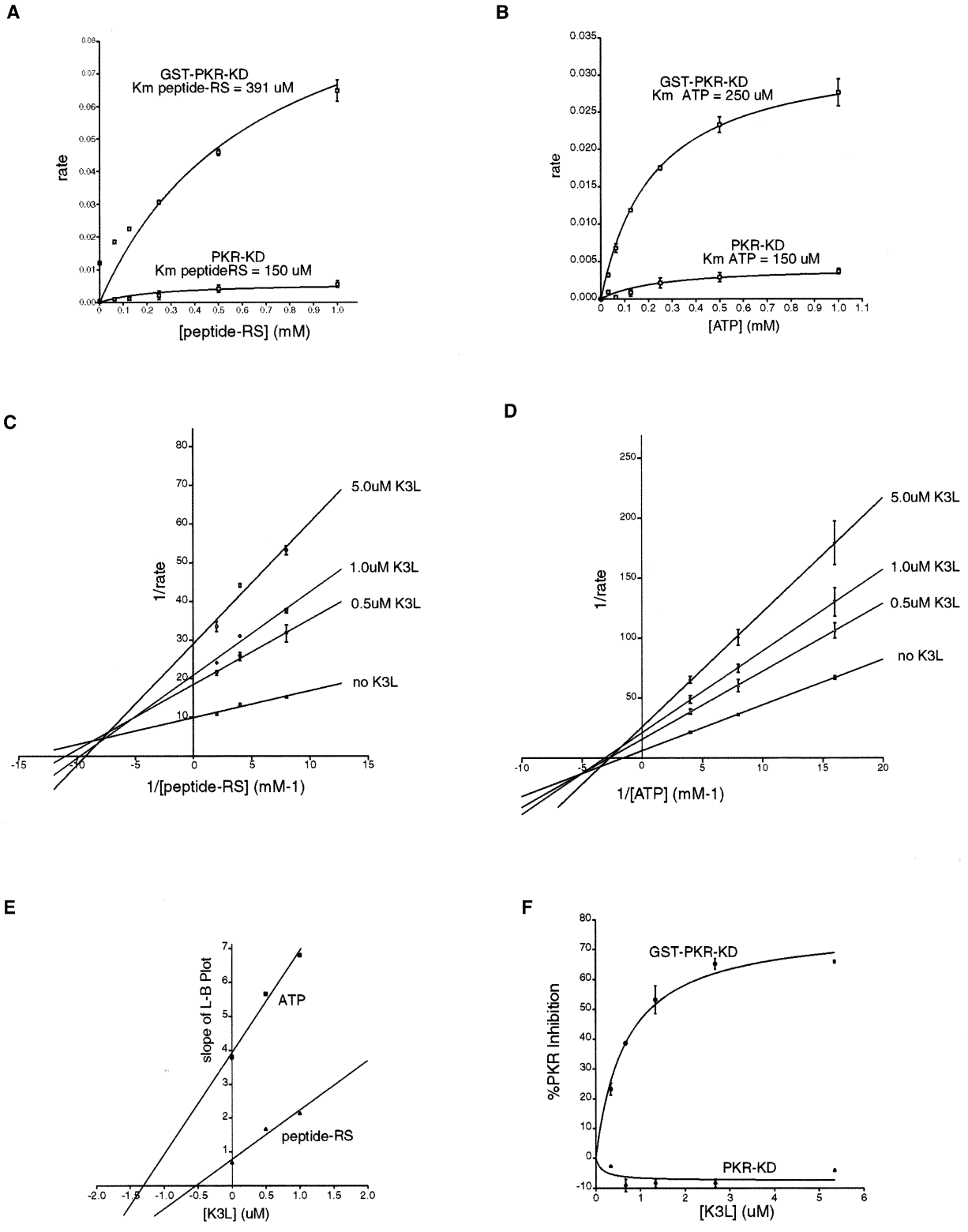

Figure 5. Kinetic Analysis of PKR Peptide Phosphorylation and K3L Inhibition Using the Spectrophotometric Assay

(A) 0.5 μM amounts of GST-PKR-KD and PKR-KD were incubated with increasing amounts of peptide-RS as indicated at fixed ATP (350 μM) concentration. Reaction rates were analyzed in duplicate.

(B) Kinase reactions were carried out as in (A) with the exception that peptide-RS concentration was kept fixed at 125 μM and ATP concentration was varied as indicated.

(C and D) Reaction rates were determined for 0.5 μM GST-PKR-KD as in (A) and (B), respectively, in the presence of the indicated concentrations of K3L. Reciprocal substrate concentration was plotted against reciprocal rate in Lineweaver-Burk format.

and quantitated by phosphor imaging. Phosphorimaging results were normalized versus the reaction rate in the absence of K3L and reported as percent PKR inhibition (Figure 4E). In the absence of K3L, GST-PKR-KD was approximately 8-fold more active than PKR-KD. In the presence of K3L, both autophosphorylation and histone phosphorylation were greatly reduced for GST-PKR-KD. In contrast, K3L did not inhibit autophosphorylation of PKR-KD and only weakly inhibited histone phosphorylation. These findings are consistent with dimerization mediating both the catalytic activation of PKR and its interaction with K3L. In Figure 4D, it is also apparent that K3L is a partial inhibitor of PKR with respect to histone and autophosphorylation (maximal inhibition $\cong$ 65% and 75%, respectively). This result is indicative of a noncompetitive mode of inhibition.

We then tested the ability of K3L to inhibit the phosphorylation of a recombinant N-terminal fragment of human eIF2α (residues 8–93) expressed in bacteria. Interestingly, GST-PKR-KD phosphorylated eIF2α efficiently while PKR-KD phosphorylation of eIF2α was undetectable (Figures 4D and 4E). Even at 8-fold higher concentrations of PKR-KD, which should compensate for the lower specific activity of the enzyme, no phosphorylation of eIF2α was detectable (data not shown). K3L was a potent inhibitor of eIF2α phosphorylation by GST-PKR-KD, and in contrast to the partial inhibitory behavior observed on histone and autophosphorylation, K3L was able to completely inhibit eIF2α phosphorylation.

To determine kinetic parameters for the K3L-PKR inhibitory interaction, we employed a coupled spectrophotometric kinase assay (Barker et al., 1995) with a model peptide substrate (peptide-RS = GRSRSRSRSR; see Experimental Procedures). Peptide phosphorylation reactions were performed with varied peptide substrate concentrations and fixed ATP concentration (Figure 5A). Similar $Km_{peptide}$ values of 392 and 150 μM were obtained for GST-PKR-KD and PKR-KD respectively by nonlinear regression analysis. Phosphorylation reactions were then performed with varied ATP concentrations and fixed peptide concentration (Figure 5B). Km_{ATP} values of 250 and 150 μM were obtained for GST-PKR-KD and PKR-KD, respectively. These values differ from the 0.25 μM value reported by Vattem et al. (2001b) but are similar to Km_{ATP} values reported for other protein kinases including Src (160 μM) (Barker et al., 1995). The discrepancy in Km_{ATP} for PKR may reflect differences in assay conditions or the presence of the His412Asn point mutation in our construct. As observed with histone as a substrate, GST-PKR-KD was far more active (10-fold) than PKR-KD at saturating levels of ATP or peptide. Since Km_{ATP} and $Km_{peptide}$ parameters were marginally better for PKR-KD, we attribute the greater activity of GST-PKR-KD to the greater catalytic efficiency of the dimeric enzyme form.

The inhibitory effect of K3L on the phosphorylation reaction was then examined with respect to peptide and ATP concentration. The data for GST-PKR-KD is plotted in Lineweaver-Burk format in Figures 5C and 5D. K3L did not significantly inhibit peptide phosphorylation by PKR-KD (see Figure 5F) and hence additional data are not shown. The intercept pattern of Figures 5C and 5D indicate that K3L is a noncompetitive inhibitor with respect to both peptide and ATP binding. By plotting the slope of the Lineweaver-Burk traces versus K3L concentration, similar intercept values of 1.4 and 0.6 μM were obtained for $K_{I\text{-}K3L}$ (Figure 5E). These values are in close agreement with the binding constant obtained for the K3L/GST-PKR-KD interaction by fluorescence polarization (K_d = 0.55 μM). As observed for histone and autophosphorylation, the maximal inhibition attainable by K3L on peptide phosphorylation by GST-PKR-KD approached 70%. This partial inhibitory behavior is consistent with the noncompetitive mode of inhibition indicated by Lineweaver-Burk analysis.

To summarize, the binding and kinetic analyses shed light on three aspects of PKR function. First, the noncompetitive behavior of K3L with respect to ATP and peptide substrate binding and the partial inhibitory effect of K3L on peptide, histone, and autophosphorylation indicate that K3L binds to PKR at a site distinct from the canonical peptide and ATP binding sites. Second, K3L's ability to completely inhibit PKR phosphorylation of eIF2α is consistent with K3L and eIF2α sharing a common binding site on PKR (i.e., a competitive mode of inhibition). Third, dimerization composes a potent switch for PKR's intrinsic catalytic activity and for its ability to recognize its natural substrate eIF2α and the pseudosubstrate K3L.

K3L Mutational Analysis

To probe the functional properties of K3L further, we generated a number of site-directed mutants and tested each for PKR inhibitory function using the peptide phosphorylation assay. All residues selected for mutation were solvent exposed in the K3L crystal structure. Mutations generated include Ile68Gln, Arg69Ala, Asp71Ala, and Tyr76Lys in the PKR recognition motif and Val44Gln, His47Gln, His47Asp, and Val52Lys in the helix insert region. Additional mutants, including Phe4Ala, Val14Gln, Tyr29Gln, His35Lys, Glu37Ala, and Tyr72Lys, were generated to provide a uniform and unbiased coverage of the K3L surface (Figures 6A and 6B). Of the 14 mutants expressed in *E. coli*, 4 could not be purified (Ile68Gln, Asp71Ala, Glu37Ala, and Val14Gln), possibly due to a disruption of the protein fold.

Peptide phosphorylation in the presence of varied concentrations of K3L was measured at fixed GST-PKR-KD and peptide substrate concentrations as described for wild-type K3L. The rates were normalized versus the rate in the absence of K3L, and plotted as percent PKR inhibition versus K3L concentration (Figure 6C). Two kinetic parameters were extrapolated from these plots by nonlinear regression analysis, namely I_{max} corre-

(E) The slope of Lineweaver-Burk traces in (C) and (D) were plotted as a function of K3L concentration. −Ki was determined as the *x*-intercept of the plots.

(F) Kinase activity of 0.5 μM GST-PKR-KD and PKR-KD in the presence of 125 μM peptide-RS, 500 μM ATP, and the indicated concentrations of K3L. Reaction rates were normalized versus the rate measured in the absence of K3L and reported as percent PKR inhibition.

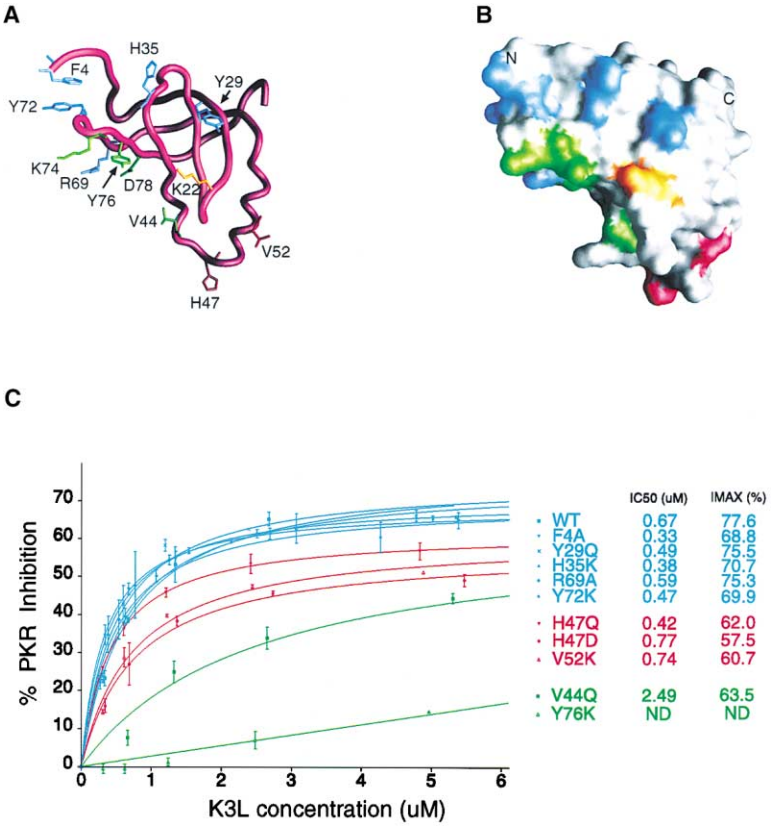

Figure 6. Functional Characterization of K3L Mutants

(A) Worm depiction of the K3L structure with the side chain of residues colored red, green, or blue according to their functional properties determined in (C). Additional residues identified as important for K3L inhibitory function (Kowagishi-Kobayashi et al., 1997), including Lys74 and Asp78 (colored green) in the PKR recognition motif and Lys22 (colored orange) in the β1-β2 linker, are also highlighted.

(B) Molecular surface representation of K3L. Highlighted surface residues are colored as in (A).

(C) Activity of 0.5 μM GST-PKR-KD with 125 μM peptide-RS substrate and 500 μM ATP in the presence of varied amounts of K3L protein as measured by the spectrophotometric coupling assay. The percent PKR inhibition was plotted versus K3L concentration and values for I_{max} (the maximal level of inhibition) and IC_{50} (the concentration of K3L protein at one-half the maximal level of inhibition) were extrapolated using GraphPad Prism v3.0 software. The K3L proteins were grouped into three classes: (1) those with wild-type properties ($I_{max} \cong 70\%$ and $IC_{50} \cong 0.5$ μM), colored blue; (2) those with reduced I_{max} but unaffected IC_{50}, colored red; and (3) those with reduced I_{max} and increased IC_{50}, colored green.

sponding to the saturable level of PKR inhibition (~70% for wild-type K3L) and IC_{50} corresponding to the concentration of K3L required for half-maximum inhibition (~0.5 μM for wild-type K3L). The IC_{50} and I_{max} values provide relative approximations of the binding affinity of the K3L proteins for GST-PKR-KD and the efficiency of inhibition at 100% binding occupancy, respectively. Based on the two kinetic parameters, we grouped the K3L mutants into three classes: those with wild-type inhibitory properties (His35Lys, Tyr29Gln, Phe4Ala, Arg69Als, and Tyr72Lys), those with weaker binding affinities as reflected by an increase in IC_{50} (Tyr76Lys and Val44Gln), and those with decreased inhibitory efficiency as reflected by a decrease in I_{max} (Val44Gln, His47Gln, His47Asp, and Val52Lys).

The Tyr76Lys mutation, which maps to the center of the PKR recognition motif, was the most potent disrupter of PKR binding. A similar mutation, Tyr76Ala, and two others in the PKR recognition motif, Lys74Ala and Asp78Ala, were previously reported to disrupt PKR inhibitory function in a heterologous yeast system (Kawagishi-Kobayashi et al., 1997). We could not purify two other K3L mutants within the PKR recognition motif (Asp71Ala and Ile68Gln), but a fourth, Arg69Ala, had no effect on K3L function. Outside of the substrate recognition motif, the Val44Gln mutation, which locates midway between the PKR recognition motif and the apex of the helix insert region (His 47), also reduced the binding affinity of K3L for PKR. Together, these results identify the PKR recognition motif and helix 1 of the helix insert region as important determinants for high-affinity binding to PKR.

Mutations in K3L that perturb the maximum efficiency of PKR inhibition include His47Gln, His47Asp, Val52Lys, and Val44Gln. These mutations map to all three secondary structure elements of the helix insert region. Unlike the Val44Gln mutation, which perturbs both IC_{50} and I_{max}, the three other mutants did not significantly alter the binding affinity of K3L for PKR. The His47Gln and His47Asp mutations map to the apex of the helix insert region, 21.5 Å removed from the center of the PKR recognition motif, while the Val52Lys mutation maps to the midpoint of helix 2. The ability of K3L mutations to selectively reduce the efficiency of PKR inhibition without perturbing binding affinity for PKR reveals two distinct and separable functions for K3L.

Discussion

Structure, mutagenesis, and kinetic analyses identify two distinct regions of the K3L structure as important for PKR binding and inhibitory function. The two regions, approximately 20 Å apart, compose a large continuous surface on one side of the K3L structure. The first region, which we refer to as the PKR recognition motif, has been delimited by conserved residues between K3L and eIF2α homologs and by new and previously reported (Kawagishi-Kobayashi et al., 1997; Sharp et al., 1997) mutagenesis data. The motif, which includes residues Lys74, Tyr76, and Asp78, forms a highly structured epitope on the β barrel component of K3L's protein fold. As mutation of this epitope greatly diminishes the binding of K3L for PKR, we believe that the chief function of the PKR recognition motif is to promote a high-affinity inter-

action with PKR. Given that K3L and eIF2α share an equivalent PKR recognition motif, that K3L can completely inhibit eIF2α phosphorylation, and that both K3L and eIF2α require PKR dimerization for recognition, we argue that K3L inhibits PKR phosphorylation of eIF2α by a strict competitive mechanism. In the context of a virus-infected cell, this would be the primary means by which K3L subverts PKR's ability to arrest cellular translation.

A second component of the K3L structure with functionally distinct properties is the helix insert region. Based on sequence and structural similarities between K3L, the S1 RBD, and eIF2α, we predict that the helix insert region adopts a unique conformation and serves divergent functions in the PKR substrate and inhibitor protein classes. In K3L, the helix insert region possesses PKR inhibitory properties, while in eIF2α, this region contains the key phosphoacceptor site implicated in translational control. Mutations in the helix insert region of K3L, including His47Gln, His47Asp, and Val52Lys, do not significantly perturb the binding affinity of K3L for PKR, but have pronounced effects on K3L's ability to noncompetitively inhibit PKR phosphorylation of short peptide substrates. As PKR has been implicated in signaling pathways that may act independent of translational control through the phosphorylation of substrates that share no structural similarity to eIF2α (reviewed in Williams, 2001), we speculate that this property of K3L may be a relevant component of its biological function.

eIF2α/K3L Binding Model

The requirement of PKR dimerization for substrate recognition and the structural model of eIF2α shown in Figure 2C provide clues as to the nature and location of the eIF2α /K3L-specific binding site in PKR. The requirement of PKR dimerization is consistent with two models of substrate recognition. In the first model, a single molecule of eIF2α binds to an extended surface spanning two PKR molecules within a productive dimer, whereas in the second model, a single molecule of eIF2α binds exclusively to a single molecule of PKR but to a surface that is allosterically regulated by dimerization. While our current data cannot resolve which of the two models (or mixture in between) is correct, our observation that the intrinsic catalytic activity of PKR is greatly enhanced by dimerization lends credence to an allosteric component to PKR dimerization. The 21.5 Å separation between the PKR recognition motif and the phospho-acceptor group Ser51 in eIF2α provides a constraint for localizing the eIF2α/K3L-specific binding site in PKR. Since the phospho-acceptor group must engage the canonical peptide binding site of PKR, the PKR recognition motif is predicted to engage a site positioned 21.5 Å away, either within the same or opposing PKR molecule of a productive PKR dimer.

The observation that K3L can noncompetitively inhibit PKR phosphorylation of histone and short peptide substrates raises the question as to how K3L exerts this effect. Since eIF2α and K3L share an equivalent PKR recognition motif, this component of the K3L structure is not expected to play a role in catalytic inhibition. Indeed, our mutational analysis implicates the helix insert region of K3L in this function. Since a common mode of binding should orient the helix insert region of both K3L and eIF2α in close proximity to the active site of PKR, the helix insert region of K3L would be well placed to impinge on catalytic function. We posit that molecular interactions involving the helix insert region of K3L perturb the local conformation of PKR's catalytic structure. Based on our kinetic analyses, we rule out the ATP and peptide binding sites as the principle targets of interference. A more detailed understanding of PKR substrate recognition and K3L inhibition awaits the structure of the PKR-K3L complex.

The Coupling of Catalytic Activation with Substrate Recognition

The coordination of substrate recognition with catalytic activation is a recurring theme in protein kinase regulation that may afford a tighter measure of control of the downstream kinase signaling response. The TGFβ and Eph receptor kinases for example, which regulate cell proliferation in response to extracellular signals, employ phosphorylation at sites within their juxtamembrane regions as a switch to couple these two activities. In the absence of phosphorylation, the juxtamembrane region of both receptors participates in the formation of a catalytically repressed state (Huse et al., 1999, 2001; Wybenga-Groot et al., 2001). Phosphorylation of the juxtamembrane region up-regulates catalytic function by relieving conformational distortions in the catalytic domain imposed by juxtamembrane association. Once dissociated from the catalytic domain, the juxtamembrane region of both receptors then acts to recruit downstream substrates through phospho-specific interactions.

In a PKR signaling response, PKR dimerization mediated by the binding of viral dsRNA would function as the analogous switch for coupling PKR catalytic activation and the recognition of eIF2α substrate. As PKR activation leads to the repression of translation, the induction of apoptosis and the transcription of proinflammatory genes, the need for a failsafe mechanism of control is evidently acute. If however, mechanisms were available to uncouple PKR's catalytic activation from the recognition of eIF2α, great potential would also exist for diversifying the nature of PKR's downstream signaling response.

Experimental Procedures

Protein Expression, Mutagenesis, and Purification

Expression and purification of the selenomethionyl derivative of K3L was performed as described (Carroll et al., 1993) with the following modifications. K3L in pET11d (Novagen, Madison, WI) was transformed into *E. Coli* B834 cells and grown in minimal media supplemented with selenomethione and ampicillin. Cells were induced with 0.5 mM isopropyl-β-D-thiogalactopyranoside (IPTG) at 37°C overnight. Low-salt precipitated K3L protein was resuspended in 300 mM $MgCl_2$, 50 mM HEPES (pH 7.0), and 5 mM DTT and applied to a Superdex 75 gel filtration column (Amersham, Piscataway, NJ) at room temperature in running buffer comprised of 300 mM $MgCl_2$, 30 mM K_2HPO_4/KH_2PO_4 (pH 7.0), and 5 mM DTT for final purification.

The Quickchange kit (Stratagene, La Jolla, CA) was used to generate K3L site-directed mutants. Expression and purification of these proteins were performed as per the K3L selenomethionyl derivative, with the exception that the gel filtration column running buffer was identical to the resuspension buffer.

The kinase domain of human PKR (residues 242–551), containing a His412Asn mutation, was expressed in *E. Coli* BL21 as a GST

fusion using the pGEX 2T vector. Protein was purified by affinity chromatography using glutathione sepharose (Amersham). The fusion protein (GST-PKR-KD) was either eluted with 40 mM glutathione or cleaved with TEV protease to liberate the isolated kinase domain (PKR-KD). After concentrating, GST-PKR-KD and PKR-KD were applied to Superdex 200 and 75 gel filtration columns (Amersham), respectively, for final purification and characterization.

The amplified cDNA sequence corresponding to the S1 domain of human eIF2α (residues 8–93) was cloned into pProEx HTa (Stratagene). The 6xHis-tag fusion protein was expressed in BL21 cells, and soluble protein was purified by nickel chelate (Amersham) and gel filtration chromatography (Amersham) as described by the manufacturer.

K3L Crystallization, Data Collection, and Structure Determination

K3L was concentrated to 20 mg/ml in 300 mM $MgCl_2$, 30 mM K_2HPO_4/KH_2PO_4 (pH 7.0), and 5 mM DTT, and crystals were obtained overnight in batch. Crystallization buffer supplemented with 20% glycerol was employed for flash freezing. Crystals contain two K3L molecules per asymmetric unit and belong to the space group C2 (a = 73.0 Å, b = 49.6 Å, c = 59.9 Å, $\alpha = \gamma = 90°$, $\beta = 100.5°$). A MAD experiment was performed at the APS beamline BM 14-D (λ_1 = 0.9788 Å, λ_2 = 0.9790 Å) using a Quantum 4 ADSC CCD detector. A remote diffraction data set was collected to 1.8 Å resolution at APS beamline BM 14-C (λ_3 = 1.0000 Å). Data processing was carried out using HKL (Otwinowski and Minor, 1997), and selenium sites were identified using CNS (Brunger et al., 1998). Experimental phase calculation and electron density map generation and modification were performed using SHARP (de La Fortelle and Bricogne, 1997). Model building and refinement were performed with O (Jones et al., 1991) and CNS (Brunger et al., 1998). In the final model, the first three and five amino acid residues of molecules 1 and 2 of the asymmetric unit respectively are disordered. No electron density for the side chains of residues 5, 86, 87, and 88 of molecule 1 and residue 6 of molecule 2 was apparent, and hence the residues were modeled as alanine.

In Vitro Binding Assay

GST and GST-PKR-KD were expressed in *E. coli* and purified by affinity chromatography using glutathione sepharose. Purified K3L proteins (20 μg) were incubated with GST and GST-PKR-KD bound to glutathione sepharose in 75 mM $MgCl_2$, 50 mM HEPES (pH 7.0), and 2 mM DTT buffer. Following extensive washing, 6$\times$ SDS-PAGE loading buffer was added, and boiled samples were subjected to 10%–20% Tris-Glycine PAGE (Novex, Invitrogen, Carlsbad, CA). Proteins were identified by coomassie blue staining, and band intensities were quantitated using Image Quant V5.0 software.

Purified, equimolar (20 μM) amounts of K3L, PKR-KD, and GST-PKR-KD alone or mixtures of PKR-KD and K3L or GST-PKR-KD and K3L were applied to 24 ml Superdex75 or Superdex200 gel filtration columns equilibrated in 75 mM $MgCl_2$, 50 mM HEPES (pH 7.5), and 3 mM DTT. 20 μl samples of column fractions were mixed with SDS load dye, applied to 10%–20% Tris gradient gels, and coomassie stained. Elution volumes of K3L ($V_{elution\_Superdex75}$ = 15.5 ml; $V_{elution\_Superdex200}$ = 19.6 ml), PKR-KD ($V_{elution\_Superdex75}$ = 9.8 ml), and GST-PKR-KD ($V_{elution\_Superdex200}$ = 12.1 ml) were significantly different such that coelution of K3L with PKR proteins was interpreted as a direct binding interaction.

Fluorescence Polarization Assay

Wild-type K3L and the Tyr76Lys K3L mutant were derivatized on cysteine residues with iodoacetamidofluorocein (Molecular Probes, Eugene, OR). 50 nM amounts of labeled K3L were incubated with varying amounts of either PKR-KD or GST-PKR-KD in 100 mM $MgCl_2$, 50 mM HEPES (pH 7.0), and 2 mM DTT. Binding reactions were completed in duplicate, and measurements were carried out on a Beacon 2000 Fluorescence Polarization System (Pan Vera, Madison, WI) at 22°C. The specific binding signal was calculated as the difference between fluorescence polarization measurements of binding reactions carried out in the absence and presence of 100-fold molar excess of unlabeled K3L. The polarization values were normalized to a common baseline and binding parameters were obtained using GraphPad Prism v3.0 software.

In Vitro Kinase Reactions

GST-PKR-KD or PKR-KD was diluted in kinase reaction buffer (17 mM $MgCl_2$, 60 mM HEPES [pH 7.0], 0.2 mM DTT) and then incubated with 7.5 μg of histone 2a and varying amounts of K3L in the presence of 100 μM cold ATP supplemented with 5 μCi of γ^{32}P ATP at room temperature in a 30 μl reaction volume. After 25 min, samples were mixed with 6 μl of 6$\times$ SDS loading buffer, boiled, and electrophoresed on 17% SDS polyacrylamide gels (Novex, Invitrogen). The gels were fixed, dried, and exposed to a Storm phospho-imager. Gels were analyzed using Image Quant v5.0 software.

GST-PKR-KD or PKR-KD was diluted in kinase reaction buffer (17 mM $MgCl_2$, 60 mM HEPES [pH 7.0], 0.2 mM DTT) and then incubated with equimolar amounts of purified His-tagged eIF2α recombinant protein and varying amounts of K3L in the presence of 500 μM ATP. After 25 min, samples were mixed with 6 μl of 6$\times$ SDS loading buffer, boiled, and electrophoresed on 4%–20% Tris-Glycine gels (Novex), transferred onto a polyvinylidene difluoride membrane (Amersham), blotted with anti-phospho-Ser51 eIF2α antibody (New England Biolabs, Beverly, MA) or anti-His antibody (Qiagen, Valencia, CA), and visualized using enhanced chemiluminescence (ECL Plus; Amersham). Gels were analyzed using Quantity One v4.2 software.

Spectrophotometric Coupling Assay

Kinetic analyses of GST-PKR-KD and PKR-KD in the presence and absence of K3L were performed using a spectrophotometric kinase assay with a model peptide substrate (peptide-RS = NH_2-GRSRSRSRSR-COOH). In this assay, the production of ADP is coupled to the oxidation of NADH through pyruvate kinase and lactate dehydrogenase, and NADH consumption is monitored directly by UV spectrophotometry at 340 nm (Barker et al., 1995). Reaction volumes (100 μl) contained 3 U lactate dehydrogenase, 3 U pyruvate kinase, 1 mM phosphoenolpyruvate, 0.2 mM NADH, 17 mM $MgCl_2$, 0.1 mM DTT, 60 mM HEPES (pH 7.0), 20 μg/ml bovine serum albumin, and varied concentrations of PKR, ATP, peptide, and K3L. In a typical analysis, protein kinase activity is linear from the start of the reaction until all NADH is consumed. The overall rate of reaction is determined as the slope of the decreasing phase of the reaction. Each data point was collected in duplicate, and pertinent kinetic parameters were obtained using GraphPad Prism v3.0 software. For GST-PKR-KD, low-level ATPase activity was observed in the absence of peptide. This may contribute to an overestimation of binding affinity. Wild-type K3L protein concentration was determined by UV spectrometry at 280 nm using a molar extinction coefficient (ϵ = 14080 M^{-1} cm^{-1}; A_{280nm} 0.1% = 1.334), and the concentrations of mutant K3L proteins were determined using the Bradford assay with wild-type K3L as a standard.

Acknowledgments

We thank Gerry Gish, Jun Liu, Joses Jones, Cheryl Arrowsmith, and Gwan-Su Yi for technical assistance with the K3L-PKR binding and K3L refolding experiments. We specially thank Glen Barber for helpful discussion and for providing PKR and K3L reagents that allowed us to initiate this project. We thank the BioCars staff at the Advanced Photon Source at Argonne National Laboratories, where diffraction data were collected. We thank Mike Tyers and Dan Durocher for helpful discussions during the preparation of this manuscript. This work was supported by grants from the National Cancer Institute of Canada. F.S. is a recipient of a National Cancer Institute of Canada Scientist award.

Received: February 19, 2002
Revised: June 19, 2002

References

Barker, S.C., Kassel, D.B., Weigl, D., Huang, X., Luther, M.A., and Knight, W.B. (1995). Characterization of pp60c-src tyrosine kinase activities using a continuous assay: autoactivation of the enzyme is an intermolecular autophosphorylation process. Biochemistry *34*, 14843–14851.

Beattie, E., Tartaglia, J., and Paoletti, E. (1991). Vaccinia virus-

encoded eIF-2 alpha homolog abrogates the antiviral effect of interferon. Virology *183*, 419–422.

Beattie, E., Paoletti, E., and Tartaglia, J. (1995). Distinct patterns of IFN sensitivity observed in cells infected with vaccinia K3L- and E3L- mutant viruses. Virology *210*, 254–263.

Brunger, A.T., Adams, P.D., Clore, G.M., Gros, P., Grosse-Kuntsleve, R.W., Jiang, J.S., Kuszewski, J., Nilges, M., Pannu, N.S., Read, R.J., et al. (1998). Crystallography and NMR system: a new software suite for macromolecular structure determination. Acta Crystallog. D *54*, 905–921.

Bycroft, M., Hubbard, T.J., Proctor, M., Freund, S.M., and Murzin, A.G. (1997). The solution structure of the S1 RNA binding domain: a member of an ancient nucleic acid-binding fold. Cell *88*, 235–242.

Carroll, K., Elroy-Stein, O., Moss, B., and Jagus, R. (1993). Recombinant vaccinia virus K3L gene product prevents activation of double-stranded RNA-dependent, initiation factor 2 alpha-specific protein kinase. J. Biol. Chem. *268*, 12837–12842.

Cosentino, G.P., Venkatesan, S., Serluca, F.C., Green, S.R., Mathews, M.B., and Sonenberg, N. (1995). Double-stranded-RNA-dependent protein kinase and TAR RNA-binding protein form homo- and heterodimers in vivo. Proc. Natl. Acad. Sci. USA *92*, 9445–9449.

Craig, A.W., Cosentino, G.P., Donze, O., and Sonenberg, N. (1996). The kinase insert domain of interferon-induced protein kinase PKR is required for activity but not for interaction with the pseudosubstrate K3L. J. Biol. Chem. *271*, 24526–24533.

Davies, M.V., Elroy-Stein, O., Jagus, R., Moss, B., and Kaufman, R.J. (1992). The vaccinia virus K3L gene product potentiates translation by inhibiting double-stranded-RNA-activated protein kinase and phosphorylation of the alpha subunit of eukaryotic initiation factor 2. J. Virol. *66*, 1943–1950.

Davies, M.V., Chang, H.W., Jacobs, B.L., and Kaufman, R.J. (1993). The E3L and K3L vaccinia virus gene products stimulate translation through inhibition of the double-stranded RNA-dependent protein kinase by different mechanisms. J. Virol. *67*, 1688–1692.

de La Fortelle, E., and Bricogne, G. (1997). Maximum-likelihood heavy-atom parameter refinement for multiple isomorphous replacement and multiwavelength anomalous diffraction methods. Methods Enzymol. *276*, 472–494.

Dever, T.E. (2002). Gene-specific regulation by general translation factors. Cell *108*, 545–556.

Gale, M., Jr., Tan, S.L., Wambach, M., and Katze, M.G. (1996). Interaction of the interferon-induced PKR protein kinase with inhibitory proteins P58IPK and vaccinia virus K3L is mediated by unique domains: implications for kinase regulation. Mol. Cell. Biol. *16*, 4172–4181.

Gribskov, M. (1992). Translational initiation factors IF-1 and eIF-2 alpha share an RNA-binding motif with prokaryotic ribosomal protein S1 and polynucleotide phosphorylase. Gene *119*, 107–111.

Hovanessian, A.G., and Kerr, I.M. (1979). The (2′-5′) oligoadenylate (pppA2′-5′A2′-5′A) synthetase and protein kinase(s) from interferon-treated cells. Eur. J. Biochem. *93*, 515–526.

Huse, M., Chen, Y.G., Massague, J., and Kuriyan, J. (1999). Crystal structure of the cytoplasmic domain of the type I TGF beta receptor in complex with FKBP12. Cell *96*, 425–436.

Huse, M., Muir, T.W., Xu, L., Chen, Y.G., Kuriyan, J., and Massague, J. (2001). The TGF beta receptor activation process: an inhibitor- to substrate-binding switch. Mol. Cell *8*, 671–682.

Johnson, L.N., Lowe, E.D., Noble, M.E., and Owen, D.J. (1998). The Eleventh Datta Lecture. The structural basis for substrate recognition and control by protein kinases. FEBS Lett. *430*, 1–11.

Jones, T.A., Zou, J.Y., Cowan, S.W., and Kjeldgaard, M. (1991). Improved methods for binding protein models in electron density maps and the localization of errors in these models. Acta Crystallogr. A *47*, 110–119.

Kawagishi-Kobayashi, M., Silverman, J.B., Ung, T.L., and Dever, T.E. (1997). Regulation of the protein kinase PKR by the vaccinia virus pseudosubstrate inhibitor K3L is dependent on residues conserved between the K3L protein and the PKR substrate eIF2alpha. Mol. Cell. Biol. *17*, 4146–4158.

McTigue, M.A., Williams, D.R., and Tainer, J.A. (1995). Crystal structures of a schistosomal drug and vaccine target: glutathione S-transferase from Schistosoma japonica and its complex with the leading antischistosomal drug praziquantel. J. Mol. Biol. *246*, 21–27.

Mellor, H., and Proud, C.G. (1991). A synthetic peptide substrate for initiation factor-2 kinases. Biochem. Biophys. Res. Commun. *178*, 430–437.

Nicholls, A., Sharp, K.A., and Honig, B. (1991). Protein folding and association: insights from the interfacial and thermodynamic properties of hydrocarbons. Proteins *11*, 281–296.

Nonato, M.C., Widom, J., and Clardy, J. (2002) Crystal structure of the N-terminal segment of human eukaryotic translation initiation factor 2alpha. J. Biol. Chem. *277*, 17057–17061.

Otwinowski, Z., and Minor, W. (1997). Processing of X-ray diffraction data collected in oscillation mode. Methods Enzymol. *276*, 307–326.

Qian, W., Zhu, S., Sobolev, A.Y., and Wek, R.C. (1996). Expression of vaccinia virus K3L protein in yeast inhibits eukaryotic initiation factor-2 kinase GCN2 and the general amino acid control pathway. J. Biol. Chem. *271*, 13202–13207.

Sharp, T.V., Witzel, J.E., and Jagus, R. (1997). Homologous regions of the alpha subunit of eukaryotic translational initiation factor 2 (eIF2alpha) and the vaccinia virus K3L gene product interact with the same domain within the dsRNA-activated protein kinase (PKR). Eur. J. Biochem. *250*, 85–91.

Sood, R., Porter, A.C., Ma, K., Quilliam, L.A., and Wek, R.C. (2000). Pancreatic eukaryotic initiation factor-2alpha kinase (PEK) homologues in humans, Drosophila melanogaster and Caenorhabditis elegans that mediate translational control in response to endoplasmic reticulum stress. Biochem. J. *346*, 281–293.

Stark, G.R., Kerr, I.M., Williams, B.R., Silverman, R.H., and Schreiber, R.D. (1998). How cells respond to interferons. Annu. Rev. Biochem. *67*, 227–264.

Ung, T.L., Cao, C., Lu, J., Ozato, K., and Dever, T.E. (2001). Heterologous dimerization domains functionally substitute for the double-stranded RNA binding domains of the kinase PKR. EMBO J. *20*, 3728–3737.

Vattem, K.M., Staschke, K.A., and Wek, R.C. (2001a). Mechanism of activation of the double-stranded-RNA-dependent protein kinase, PKR: role of dimerization and cellular localization in the stimulation of PKR phosphorylation of eukaryotic initiation factor-2 (eIF2). Eur. J. Biochem. *268*, 3674–3684.

Vattem, K.M., Staschke, K.A., Zhu, S., and Wek, R.C. (2001b). Inhibitory sequences in the N-terminus of the double-stranded-RNA- dependent protein kinase, PKR, are important for regulating phosphorylation of eukaryotic initiation factor 2alpha (eIF2alpha). Eur. J. Biochem. *268*, 1143–1153.

Williams, B.R. (2001). Signal integration via PKR. Sci. STKE *89*, RE2.

Wybenga-Groot, L.E., Baskin, B., Ong, S.H., Tong, J., Pawson, T., and Sicheri, F. (2001). Structural basis for autoinhibition of the Ephb2 receptor tyrosine kinase by the unphosphorylated juxtamembrane region. Cell *106*, 745–757.

Accession Numbers

Coordinates have been deposited with the Protein Data Bank, ID code 1LUZ.